Effect of sidewall on the flame extension characteristics beneath a ceiling induced by carriage fire in a channel

Fei Tang[a], Peng Hu[a], Qing He[a], Jianping Zhang[b], Jennifer Wen[c,*]

[a] School of Automotive and Transportation Engineering, Hefei University of Technology, Hefei, Anhui 230009, China

[b] FireSERT, Belfast School of Architecture and the Built Environment, University of Ulster, Newtownabbey, BT37 0QB, United Kingdom

[c] School of Engineering, University of Warwick, Coventry CV4 7AL, United Kingdom

Corresponding author:

Jennifer Wen

School of Engineering

University of Warwick

Coventry CV4 7AL, UK

Phone: +44 (0)24 765 73365

Email address: Jennifer.wen@warwick.ac.uk

Abstract

Laboratory tests were firstly conducted in a reduced scale channel to investigate the conditions for flame ejections when the carriage was at the centre of the channel. The ejected flames were recorded by two cameras and the temperature inside the enclosure and on the ceiling were measured. The lower critical heat release rate (HRR) which would result in intermittent flame ejection and upper critical HRR which would lead to continuous external flame were analysed with regards to their variations with the ventilation factor. Correlations for the longitudinal and transverse flame extension lengths and flame extension area beneath the ceiling were proposed. Subsequently further experimental investigations were conducted to study the effect of sidewall constraint on flame extension by changing the position of the carriage along the transverse direction to vary the distance between the sidewall and the carriage opening, which was also systematically varied. With the decrease of the sidewall-to-opening distance, the longitudinal flame extension length was found to increase whereas the transverse flame extension length decreased. The changes are most significant when sidewall-to-opening distance was relatively small. These trends are different from those observed in previous wall-attached fires or corner fires in channels, where the flame extension length beneath the ceiling firstly increased with the decrease of sidewall-source distance, and then decreased slightly when the fire source was attached to the wall. New correlations were proposed to account for the effect of sidewall-to-opening distance for longitudinal and transverse flame extension lengths under the ceiling. They captured well the measurements for all the present cases and some published cases not used in their derivation, demonstrating the potential for fire safety engineering applications.

Keywords: Flame extension; Channel fire; Sidewall; Carriage fire; Ejected flame; Ceiling jet.

Nomenclature

A	opening area (m^2)	$m_{entrainment}$	air entrainment mass rate (kg/s)
A_T	total exposed surface area of the enclosure excluding the opening (m^2)	$\dot{Q}$	total heat release rate (kW)
c_p	specific heat of air at constant pressure (kJ/kg·K)	$\dot{Q}_{inside}$	maximum theoretical heat release rate consumed inside the compartment (kW)
C_1	a parameter related to air entrainment.	$\dot{Q}_{ex}$	excess heat release rate (kW)
C_2	a parameter related to air entrainment.	$\dot{Q}^*_{ex}$	dimensionless excess heat release rate
D	Sidewall-to-opening distance (m)	S	flame extension area (m^2)
g	gravitational acceleration (m/s^2)	$S_{entrainment}$	air entrainment area (m^2)
H	opening height of carriage (m)	S_{front}	air entrainment area from the front of the opening sizes (m^2)
ΔH_c	combustion heat of the fuel (kJ/kg)	S_{side}	air entrainment area from the side of the opening sizes (m^2)
$H_{carriage}$	height of the carriage (m)	T_f	ejected flame temperature (K)
H_f	ejected flame height for free condition without tunnel ceiling (m)	T_∞	ambient air temperature (K)
$H_{neutral}$	height of the neutral (m)	v_a	air entrainment velocity (m/s)
$\Delta H_{O\chi}$	heat release per mass of air consumed at normal conditions (3000 kJ/kg)	V_f	total volume of the ejected flame without a ceiling (m^3)
H_{tunnel}	tunnel height (m)	V_{fu}	volume of the flame intercepted by the ceiling (m^3)
k	ratio of the distance between the neutral plane and the ceiling to the distance between the carriage top and the ceiling	W	opening width of carriage (m)
K	air entrainment correction factor	Z	height from the neutral plane to the ceiling of the tunnel (m)
K_L	longitudinal air entrainment correction factor	***Greek symbols***	
K_T	transverse air entrainment correction factor	φ	ratio can be obtained by integrating, Eq. (8)

ℓ	flame extension length under the ceiling (m)	ρ_f	density of ejected flame (kg/m^3)
ℓ_1	characteristic length (m)	ρ_∞	ambient air density (kg/m3)
ℓ_2	characteristic length (m)	λ	coefficient of air entrainment due to the influence of side wall distance D
ℓ_L	longitudinal flame extension length under ceiling (cm)	λ_L	coefficient of longitudinal air entrainment
ℓ_T	transverse flame extension length under ceiling (cm)	λ_T	coefficient of transverse air entrainment
m	coefficient for constants		

1. Introduction

The construction of underground channel (e.g., underground road) has grown rapidly in recent years. This is accompanied by increasing occurrence of channel or tunnel fire accidents. For example, the Daxing underground channel fire accident in China killed 18 people in 2017. There have been growing concerns over the fire safety of long and narrow channel structure, such as tunnel, due to the increase in construction of channel or tunnel systems worldwide and recent major fire incidents. Previous studies have shown that the ceiling jet, which is created by flame impingement on the ceiling, is of critical importance to fire safety in channel and tunnels. However, previous studies were largely focused on the ceiling jet flame spread characteristics induced by free fire plumes in the tunnel [1]. A significant amount of work has also been conducted towards quantifying the ceiling flame spread characteristics [2-7] in building fires. You and Faeth [4] studied the impinging flame lengths along the horizontal ceiling and ceiling heat fluxes for both unconfined and confined ceilings, proposed an empirical flame extension length model. Ding and Quintiere [6] experimentally investigated impinging ceiling flames and proposed an integral model for flame extension lengths under the ceiling, using an empirical relationship for the mixing ratio of air entrained to the stoichiometric air needed for the

ceiling jet flame.

For the effect of sidewall on free fire plume and impinging flame under the ceiling in a channel or tunnel like construction, many previous studies considered in default that the fire is at the centre of the channel or tunnel. However, in an actual channel or tunnel-like construction fire accident, the distance between the fire source and the side wall of the channel or tunnel can vary. Such variation can significantly affect flame spread characteristics of the ceiling jet due to the resulted change in air entrainment of the confined flame. In open fires, flames entrain air in all directions [8, 9]. In the presence of sidewall restrictions, air entrainment is affected. This will result in changes in the flame height and flame extension length under the ceiling in case of flame impingement. Research along this direction has been pursued by various investigators [10-26]. Zukoski [10] studied the wall-attached fire plume assuming that there was an imaginary fire source on the other side of the wall, which had the same intensity as the original fire source. Hasemi and Tokunaga [11] studied turbulent diffusion flames and buoyant plumes from fire sources against a wall and in a corner of walls; and found that the sidewall had considerable effect on the flame height and temperature. Poreh and Garrad [12] carried out experiments with the fire source close to a wall or having a certain distance from the wall. Their study reveals that air entrainment into the fuel laden fire flames is reduced and the burning of the fuel is completed at higher heights. Takahashi and Tanaka [13] also conducted experiments to investigate the relationship between air entrainment and flame/plume behaviour when a fire source was placed in and near a corner of vertical walls. Recently, Tang et al. [16] conducted experiments to study the effect of cross wind on near-wall buoyant turbulent diffusion flame length and tilt angle, it was found that the mean flame length of near-wall burning was significantly higher than that of middle flame (free burning) for a given source heat release rate and cross-wind speed, which indicated appreciable air

entrainment differences between near-wall flame and free burning. Ji et al. [17] investigated the sidewall effect on flame characteristics and burning rate of n-heptane pool fires. It was found that, due to air entrainment restricted by the sidewall, the vertical flame volume decreased and ceiling flame length increased. Zeinali et al. [21-22] experimentally tested fires in the corners of the walls and found flame height being affected by the restricted air entrainment. Zhang et al. [25] examined flame extension length in different directions under the inclined ceiling, and found that as the inclination angle increased, the longitudinal flame extension length decreased, and the transverse flame extension length increased. For flat ceiling, the length of the longitudinal flame was greater than that in the transverse direction. Therefore, when moving the fire source close to the side wall, the longitudinal and transverse flame extension length under the ceiling will change due to the restricted air entrainment. This effect has implications on fire safety and hence warrant quantification. There is also the need for simple correlations to cater for such scenarios for fire safety engineering applications.

Another very important phenomenon in channel or tunnel-like construction fires is the ejected flame from under-ventilated carriage fires, which could cause damage to the channel or tunnel structure. Whilst much research has been conducted on the ejected flame from an enclosure in building fires [27-30], relatively little research has been undertaken for channel or tunnel-like construction fires. In a collision accident, large goods or container vehicles could catch fire, resulting in ceiling flame spread if the heat release rate is sufficiently high because of large number of flammable objects. such as, Lee et al. [27] correlated the ejected flame height with the excess heat release rate outside the enclosure ($\dot{Q}_{ex}$) by assuming that the ejected thermal plume from the enclosure opening can be physically approximated as a rectangular fire source against the facade wall with two characteristic lengths of $\ell_1 = (AH^{1/2})^{2/5}$ (parallel to the facade wall) and $\ell_2 = (AH^2)^{1/4}$ (normal to the facade wall), where A

is the opening area and H is the height of opening. Note that the heat release rate inside the enclosure for under-ventilated fire conditions can be estimated as $\dot{Q}_{in} = 1500A\sqrt{H}$ [27, 31, 32].

In summary, insight into the characteristics of ceiling jets caused by ejected flames from carriages in channel or tunnel-like structured is still lacking. Particularly, no research has been conducted to address the effects of sidewall to carriage distance (the distance between tunnel sidewall and carriage opening) on the ceiling flame spread characteristics in channel or tunnel-like structure fires, and the related safety implications. In such scenarios, due to air entrainment restrictions, the heat release rate (HRR) inside the enclosure may change with sidewall to carriage distance, and consequently the flame extension of the ceiling jet changes accordingly and the resulting fire hazard. The present study aims to filling these knowledge gaps through experimental investigations and provide some simplified formulas which can be used in fire safety design.

2. **The experimental setup**

A series of laboratory tests were conducted in a reduced-scale model channel or tunnel-like structure (1:8) of 22 m (L) × 1.2m (W) × 0.8 m (H) as shown in Fig. 1. Based on the Froude similarity criterion, $\dot{Q}_M = \dot{Q}_F(1/8)^{5/2}$, (M is the model experiment, F is the full scale tunnel main channel), The corresponding full-size channel or tunnel-like structure section is 9.6 m (W) × 6.4 m (H) [33]. The floor of the model channel or tunnel-like structure is made of steel plates, which are covered by temperature resistant material. One sidewall is made of reinforced transparent glass while the other sidewall and the ceiling are made of glass magnesium board. The ambient temperature was about 16±4℃ in all tests.

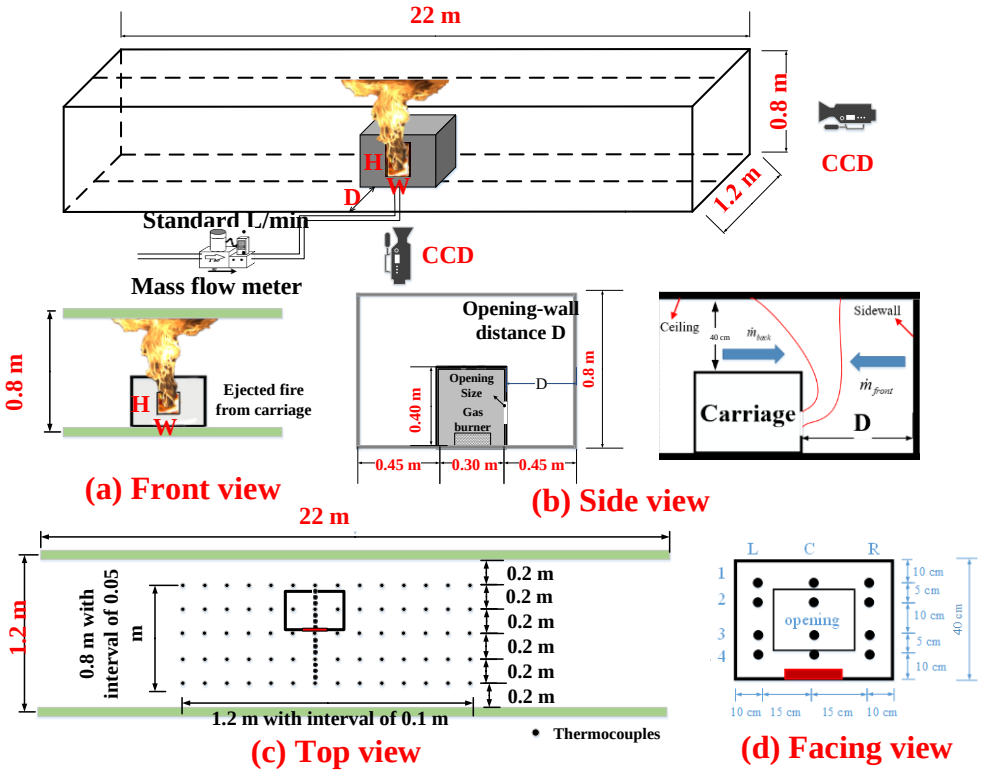

Figure 1 Schematic diagram of the experimental device.

Table 1. Experimental conditions for external flames

Openings size		Side wall-Opening	HRR (kW)
H (cm)	*W* (cm)	distance *D* (cm)	
10	15	60, 50, 40, 30, 25, 20	50.4, 67.2, 84
15	10	60, 50, 40, 30, 25, 20	50.4, 67.2, 84
15	15	60, 50, 40, 30, 25, 20	50.4, 67.2, 84
20	10	60, 50, 40, 30, 25, 20	50.4, 67.2, 84

The model scale carriage is 0.5 m (L) × 0.30 m (W) × 0.40 m (H). It is made of 3 mm thick steel plates and 10 mm thick fireproofing boards. A porous propane gas burner was placed at the centre flush with the carriage floor. The fuel flow rate is controlled by a mass flow meter (Alicat). Four

different opening dimensions were used to represent different aspect ratios and ventilation factors. The distance between the sidewall of the channel or tunnel-like structure, the opening of the carriage and the heat release rate (HRR) were systematically varied. In order to select the appropriate HRRs to facilitate examinations of flame extensions under the ceiling, the critical HRR which can result in external burning was firstly studied with the carriage under open conditions by varying the HRR from 4.4 kW to 40 kW. These results are analysed in Section 3.1. Subsequently, the investigations were focused on studying the flame extension characteristics beneath a ceiling induced by a carriage fire in a channel or tunnel-like structure. The three HRRs used were 50.4, 67.2 and 84 kW, which were chosen to ensure that the flame impinges on the ceiling for all the opening sizes and sidewall–carriage distances. Tests were also conducted with the carriage in open conditions at the same HRRs to obtain the ejected flame height for free condition, the results of which are shown in Section 3.3. The detailed experimental conditions for the tests can be found in Table 1. According to the Froude similarity criterion of Quintiere [33], the HRRs used in the experiment are equivalent to actual fire HRRs from 9.1 MW to 15.2 MW, which is in line with the HRR of a truck or passenger car fire.

The flame evolutions were captured from the front view and side view by two charge-coupled device (CCD) cameras with a frequency of 50 frames per second. One camera was located at the right end of the channel to record the transverse flame development and the other perpendicular to the fire-resistant glass side wall to record the longitudinal flame evolution. The transverse and longitudinal flame extensions beneath the channel ceiling were determined through image processing. As shown in Fig. 2, the original flame image was firstly converted to grey-scale image, and next to binary image using the Otsu method [32, 34] through MATLAB program. Flame intermittency distribution was then obtained by averaging the values of these consecutive binary images in each pixel position. Finally,

the flame intermittency distribution contour was used to represent one experimental case to obtain the mean flame dimension values at intermittency p= 0.5.

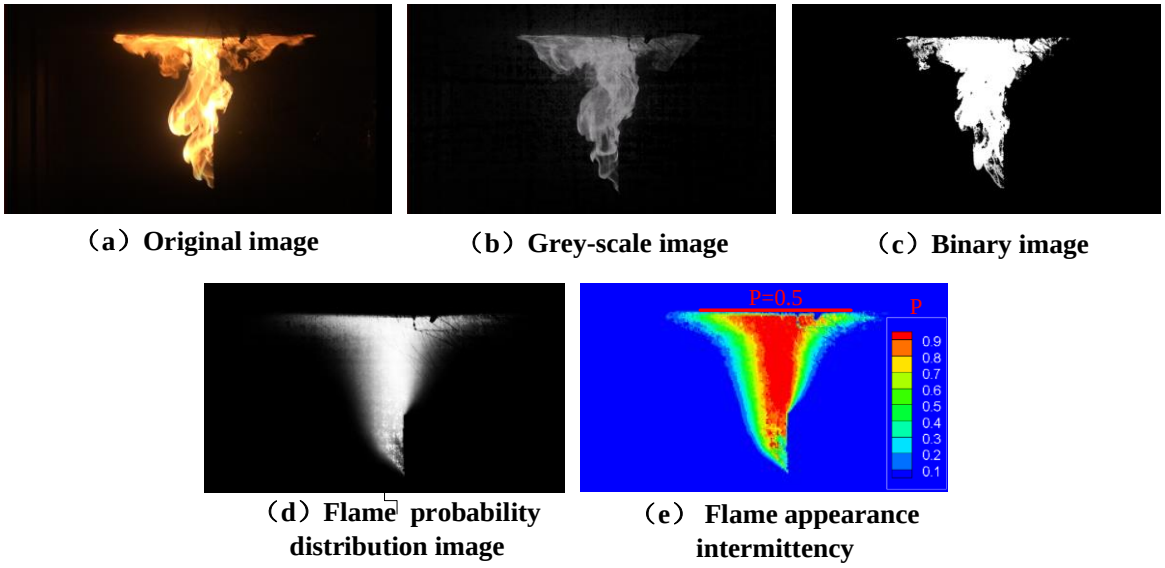

（a）Original image　（b）Grey-scale image　（c）Binary image

（d）Flame probability distribution image　（e） Flame appearance intermittency

Figure 2. Definition of the flame extension length based on image processing.

For temperature measurements, several K-type thermocouple arrays were placed under the ceiling, covering an area of 1.2 m in length with 0.1 m interval and 0.8 m in width with 0.2 m interval. Additional thermocouples were arranged along the transverse centreline with 0.05 m spacing between them as shown in Fig. 1c. In the vertical direction, three thermocouple trees of 4 thermocouples each, were arranged, in the centre and 10 cm from the left and right side walls with the first thermocouple 10 cm under the ceiling and 5 cm spacing between the adjacent ones as shown in Fig. 1d. Another thermocouple was placed at the centre of the opening to measure the ejected flame temperature.

Most of the thermocouples have a diameter of 1 mm. Two additional thermocouples with diameters of 0.5 mm and 1.5 mm were also used to estimate radiation errors following Blevin and Pitts [35]. It was found that the resulting correction increased with the increase of the measured temperature. The uncertainty range of the thermocouple measurements was estimated to be less than 5% in the hot gas layer.

Table 2 Estimation of uncertainties: example of measured longitudinal flame extension length (ℓ_L) and transverse flame extension length (ℓ_T). (*D*=60 cm)

Quantities	Opening size *H**W* (cm*cm)	Heat release rate (kW)	Repeat test 1 (X_1) (cm)	Repeat test 2 (X_2) (cm)	Repeat test 3 (X_3) (cm)	Average value $\bar{X}$ (cm)	2σ (cm)	$\frac{2\sigma}{\text{Average}}$ (%)
Longitudinal flame extension length (ℓ_L)	10*15	50.4	25.49	25.11	25.24	25.28	0.32	1.26
		67.2	36.76	37.11	36.29	36.72	0.67	1.83
		84	46.39	45.51	46.79	46.23	1.07	2.31
	15*10	50.4	24.26	24.61	24.54	24.47	0.30	1.22
		67.2	39.49	40.31	40.38	40.06	0.80	2.00
		84	50.36	49.97	48.89	49.74	1.24	2.48
	15*15	50.4	19.72	19.82	19.59	19.71	0.19	0.98
		67.2	35.66	36.26	35.51	35.81	0.64	1.79
		84	48.04	46.71	47.66	47.47	1.12	2.37
	20*10	50.4	19.31	19.16	19.37	19.28	0.18	0.96
		67.2	30.42	30.98	30.76	30.72	0.47	1.53
		84	40.55	40.47	39.67	40.23	0.80	2.01
Transverse flame extension length (ℓ_T)	10*15	50.4	35.33	35.98	36.03	35.78	0.64	1.78
		67.2	47.83	47.03	46.47	47.11	1.11	2.35
		84	55.56	56.34	57.63	56.51	1.71	2.92
	15*10	50.4	39.01	38.14	38.8	38.65	0.74	1.93
		67.2	46.39	47.55	46.37	46.77	1.09	2.33
		84	51.64	51.62	50.25	51.17	1.30	2.55
	15*15	50.4	31.84	32.44	32.29	32.19	0.51	1.60
		67.2	43.05	42.42	43.56	43.01	0.92	2.15
		84	53.08	54.16	52.45	53.23	1.41	2.66
	20*10	50.4	34.87	34.16	34.59	34.54	0.59	1.72
		67.2	41.95	43.02	42.26	42.41	0.89	2.12
		84	56.98	55.24	57.13	56.45	1.71	2.92

Each test condition was repeated three times to check repeatability, and the average from the three tests were taken as the measurements. Table 2 illustrates the uncertainty analysis. Assuming X_i is the measured values of N set of repeated experiments (N = 3 here), σ is the standard unbiased deviation of repeated data, then $\sigma = \sqrt{\frac{\sum_{i-1}^{N}(X_i - \bar{X})^2}{N-1}}$. The mean value lies within the range of ± 2

σ, with confidence 95%. Table 2 gives an example of the uncertainty analysis for the different conditions for D = 60 cm. With 95% confidence, the relative uncertainty $\frac{2\sigma}{\text{Average}}$ is less than 3%. The error bars in the experimental data shown in Figs. 7 indicate that the mean values represent the overall data within an uncertainty of 3%.

3. **Results and discussion**

3.1 Flame extension length and area on the ceiling induced by ejected carriage fires at the centre of the channel

The HRR is a critical parameter for fire characterization. For under-ventilated fully involved fires in an enclosure, the mixture is fuel rich. Some unburnt fuel exit through the opening and mix with ambient air, resulting in external/ejected flame. Lee et. al. [27] conducted small-scale experiments to investigate the conditions leading to ejected fire plume from a carriage by analyzing the critical heat release rate within the enclosure and arrived at the following formula:

$$\dot{Q}_{inside} = 0.133 \frac{\Delta H_{O\chi}}{c_\rho T_\infty} c_\rho T_\infty \rho_\infty A\sqrt{gH} = 1500 A\sqrt{H}\,(kW) \tag{1}$$

where $\dot{Q}_{inside}$ is the lower critical HRR.

(a)Flame burning inside the carriage

(b) Intermittent flame ejecting behavior

(c) Flame continuously burning outside the carriage

Figure 3. Different phases of flame ejecting behaviour.

However, the actual combustion conditions in different situations may differ from that tested by Lee et al. [27], which were used to derive the above formula. It is, hence, necessary to assess the actual heat release rate to judge the propensity for flame ejection.

The flame images shown in Fig. 3 were derived from the frame captured by the CCD cameras. For each test, more than 30 s of original videos were recorded in the flame stable moment. The videos of 30 s were converted into the gray scale images, resulting in 1500 consecutive frames for each test which constitute a large data set to derive statistics with accuracy. The flame ejection probability was defined as the number of ejected flames divided by the total number of the blanket flame images.

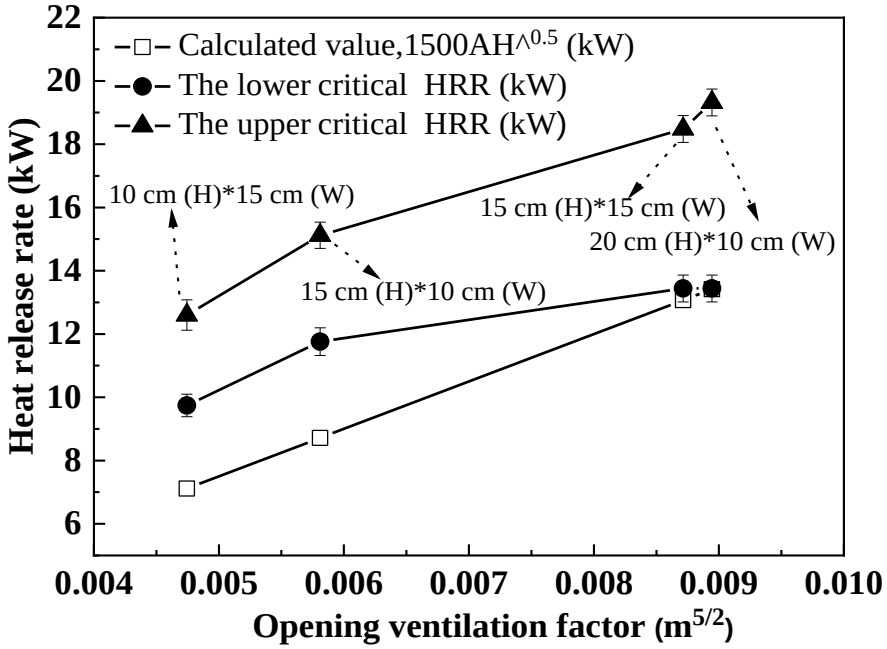

Figure 4. Comparison of the lower and upper critical HRRs with the predicted critical HRR (*D*=60 cm).

To facilitate the discussion, the flame images in Fig. 3 are divided into three burning stages following the analysis of Hu et al. [36], namely no flame ejection (where all the fuel is consumed inside the enclosure and the HRR is less than $1500A\sqrt{H}$), intermittent flame ejection (flames being ejected out intermittently with a certain probability) and continuous external flames. For the first phase shown in Fig. 3(a), in which combustion was only inside the enclosure, only hot combustion products

were ejected from the opening. Following Hu et al. [36] who investigated ejected flames from an enclosure in open space, a lower critical HRR is proposed to characterize the beginning of intermittent ejection. A higher critical HRR is additionally proposed to indicate the end of the intermittent transition regime with the flame continuously burn outside the opening. Both the lower and higher critical HRRs were found to be dependent on the ventilation factor [36]. It was also found that the lower HRR changes linearly with the parameter $A\sqrt{H}/A_T$ (where A_T is the total exposed surface area of the enclosure excluding the opening), which represents the influence of heat loss to enclosure walls on fire plume temperature. The variations of HRR with the ventilation factor are plotted in Figure 4, where the green symbols are the predicted critical HRRs [27] at the selected ventilation factors, and the red and black symbols represent the measured lower and upper critical HRRs which can result in ejected flamed. Figure 4 shows that the critical HRRs of flame ejection increased with the increase of the ventilation factor. The lower critical HRR gradually approaches the predicted critical HRR with the increase of the ventilation factor and became almost the same when the ventilation factor reached a certain value.

Figure 5 shows the temperature evolutions inside the enclosure with the opening size of 15 cm × 15 cm but varying heat release rates when the burner was placed at the centre of the channel. The figure legends R-#, C-# and L-# represents temperature measurements by the thermocouple tress shown in Fig. 1d on the right, centre and left, respectively. Hu et al. [36] have shown that the temperature inside the compartment have an important effect on the intermittent flame ejection, affecting both the ignition of the flammable mixtures and the degree of fluctuations of the ejected buoyant flames. Following Hu et al. [36], three stages can be identified in all the tested cases as shown in Fig. 5. The intermittent behaviour of flames outside the enclosure is characterized by the flame

intermittent probability, which can be obtained by processing the captured flame images for tests with different HRRs as well as lower and higher critical HRRs. The results show that (1) for the internal burning stage during fuel-control stage with no ejected flame, the temperature (left corner, right corner and the centre) inside the enclosure increases gradually with the increase of HRR; (2) for the intermittent flame ejection stage, the temperature inside the enclosure increases slowly with the increase of HRR due to incomplete combustion as a result of an increase in the fuel supply; (3) for the continuous external flames stage, the temperature remains nearly constant with any further increase of HRR as the fire has become ventilation-controlled.

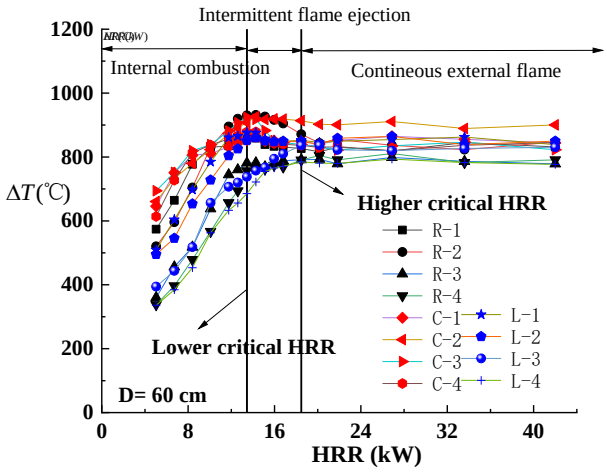

Figure 5. Temperature evolution inside the enclosure under different heat release rates when the fire at the centre of the channel (opening size is 15 cm*15 cm).

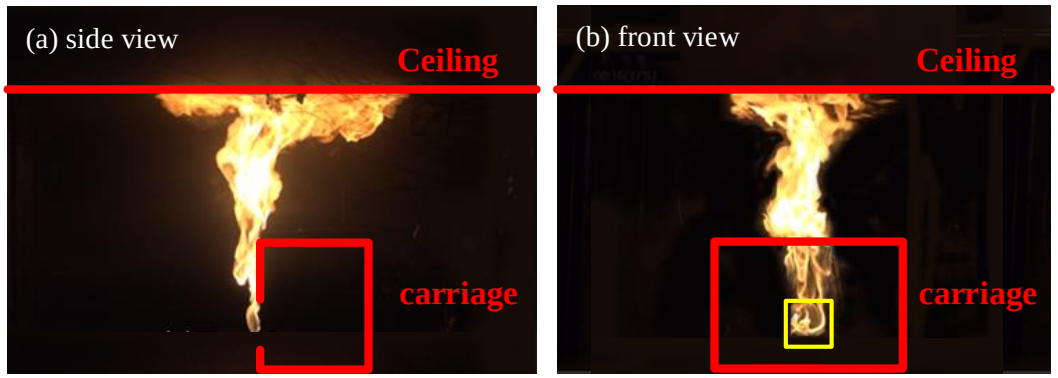

Figure 6. Flame images for the case with *D* = 60 cm (Opening size is *H*=15 cm, *W*=15 cm and HRR=67.2 kW), (a) Side view (transverse direction) (b) Front view (longitudinal direction).

Figure 6 displays the flame images of transverse and longitudinal flame extension with Side wall-Opening distance D = 60 cm (Opening size is H=15 cm, W=15 cm and HRR=67.2 kW). Due to the restriction of the sidewall, the flame upon exiting the carriage opening quickly turned upwards and propagated to reach the ceiling. The extent of its spread in the transverse direction of the channel was much larger than that in the longitudinal direction.

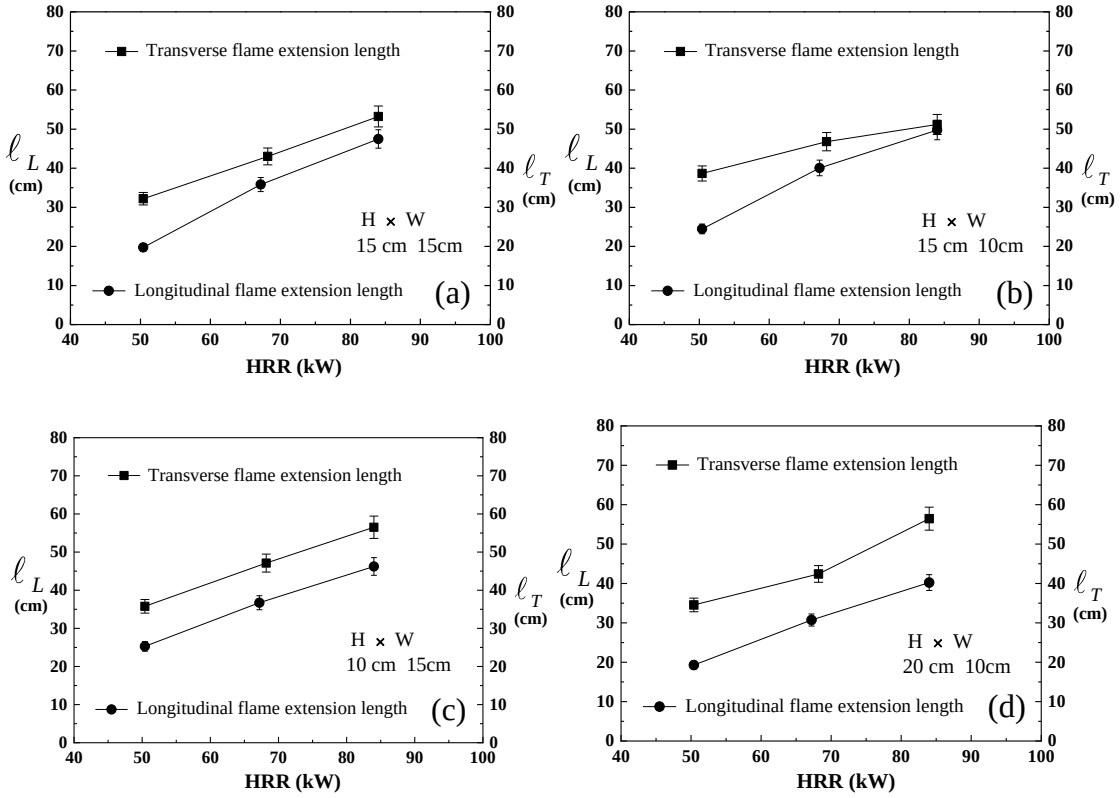

Figure 7. Flame extension lengths under the ceiling with different opening size at the centre of the channel.

Figure 7 shows the flame extension lengths under the ceiling induced by carriage fires with different opening sizes at the centre of the channel (the opening of the carriage is located at the centreline of the tunnel), where ℓ_L is the longitudinal flame extension length (cm) and ℓ_T is transverse flame extension length (cm). The flame extension length in the longitudinal direction is always lower than that in the transverse direction when the carriage fire is at the centre of the tunnel. This difference is thought to be due to fire-induced flow features as the ejected flame carries moment

in the transverse direction [8, 9, 27, and 37]. Following Lee et al. [27], the characteristic exit velocity from the opening in the transverse direction is $u \sim \sqrt{\frac{\Delta T_g}{T_\infty} gH}$, where ΔT_g the temperature rise inside the carriage and H is is the height of carriage opening. The resulting external flame hence carried moment in the transverse direction, driving the ceiling flame to extend more across the channel upon impingement and resulting in relative longer ceiling flame length.

There are some differences in the results between Figs. 7(b) and 7(d) as well as between Figs. 7(b) and 7(c). In Figs. 7(b) and (d), the opening sizes are 15 cm (height) × 10 cm (height), 20 cm (height) × 10 cm (height), respectively. The characteristic exit velocity from the opening in Fig. 7(d) is larger than that of Fig. 7(b), resulting in larger flame extension length in the transverse direction in Fig. 7(d) while the flame extension lengths in the longitudinal direction are similar. The opening area in Figs. 7 (b) and 7 (c) are the same, but the height of opening is different. As shown in Fig.4, the critical HRRs of the ejected flame increase with the increase of the ventilation factor. The critical HRRs for the opening of 10 cm (height) × 15 cm (height) is lower than the opening of 15 cm (height) × 10 cm (height), resulting in some differences between them.

The flame extension length induced by the ejected flame from a carriage in a channel should be a function of the excess HRR, i.e., $\ell + Z = fcn\left(\dot{Q}_{ex}\right)$. This expression can be normalized by the characteristic length, ℓ_1, to obtain the following dimensionless form:

$$\left(\ell + Z\right)/\ell_1 = fcn\left(\dot{Q}_{ex}/\ell_1\right) = fcn\left(\dot{Q}^*_{ex}\right) \tag{2}$$

where $\dot{Q}^*_{ex} = \dot{Q}_{ex}\Big/\left(\rho_\infty T_\infty C_p \sqrt{g}\,\ell_1^{5/2}\right)$, $\dot{Q}_{ex} = \dot{Q} - \dot{Q}_{inside}$, ℓ is flame extension length under the ceiling (m), Z is the height from the neutral plane to the ceiling of the tunnel (m), $\ell_1 = (AH^{1/2})^{2/5}$, $\dot{Q}_{ex}$ is excess heat release rate (kW), $\dot{Q}_{inside}$ is maximum theoretical heat release rate consumed inside the compartment, which can be obtained from the lower critical HRR as shown in Fig. 8, T_∞ is the ambient

temperature (K), ρ_∞ is the air density (kg/m^3), C_ρ is the specific heat of air at constant pressure (kJ/kg.K), and g is the gravitational acceleration (m/s^2).

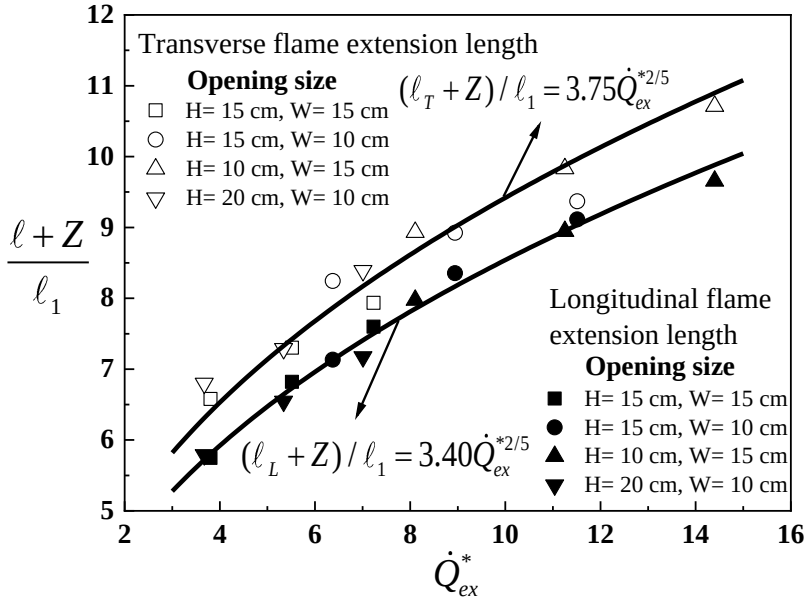

Figure 8. The dimensionless flame extension length *vs* dimensionless excess heat release rate at the channel centreline (*D* = 60 cm).

Figure 8 plots the dimensionless flame extension length against the dimensionless excess heat release rate in both longitudinal and transverse directions. The least square fit of the data shows that the flame extensions in both directions are proportional to the 2/5 power of the dimensionless excess heat release rate and the following two expressions exist:

Longitudinal flame extension length: $(\ell_L + Z)/\ell_1 = 3.40\dot{Q}^{*2/5}_{ex}$ (3a)

Transverse flame extension length: $(\ell_T + Z)/\ell_1 = 3.75\dot{Q}^{*2/5}_{ex}$ (3b)

As shown in [7], the underlying physics for the extension of a ceiling jet from an ejected flame is related to the spreading of the unburnt fuel after impingement and its continuous combustion while spreading at the ceiling. The flame extension area can be expressed as:

$$S \sim fcn\left(\frac{V_{fu}}{V_f}\dot{Q}_{ex}\right) \tag{4}$$

where $\dot{Q}_{ex}$ is the total heat release rate for an open fire source or the excess heat release rate from an

enclosure fire, V_f is the total volume of the ejected flame without a ceiling and V_{fu} is the volume of the flame intercepted by the ceiling and the term on the Right-Hand-Side (RHS) of Eq. (4) represents the HRR of the un-burnt fuel after impingement (assuming that the combustion in the flame region is uniform).

When the carriage is located at the transverse centreline, the flame length area under the ceiling can be expressed as $SV_f \in V_{fu}$, where $V_f = \sqrt{\left(\Delta T_f / T_\infty\right) gZ}$ [8, 38] and T_f is the temperature of the ejected flame.

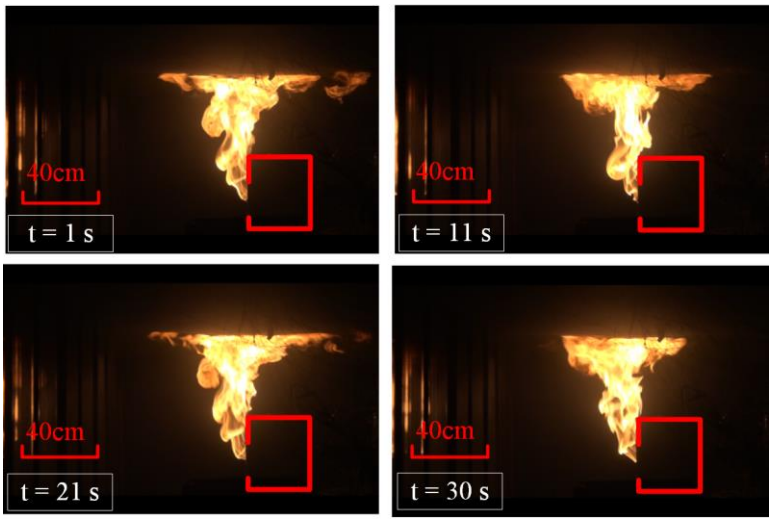

Figure 9. The flame images at different time for the case with *D* = 60 cm (Opening size is *H*=20 cm, *W*=10 cm and HRR=84 kW).

Figure 9 presents some instantaneous the flame images at different time. The shape of the upward spreading flame like a cone. Since the flames body have different extension lengths in the horizontal and vertical directions, the expansion area under the ceiling is like an ellipse [38].

Assuming that the cross section of the flame is an ellipse following Quintiere and Grove [38], the longitudinal and transverse flame extension length can be calculated by the following equation:

$$\ell_L / 2 = \ell_1 / 2 + C_1 Z \quad , \quad \ell_T / 2 = \ell_2 / 2 + C_2 Z \tag{5}$$

where the C_1, C_2 are coefficients. Due to the presence of the carriage wall and the existence of the

narrow space above the carriage top, air entrainment at the rear part of the ejected fire plume is relatively weak, and the flame extension at the ceiling tilts towards the rear direction. The coefficient C_2 can be assumed to be proportional to C_1, i.e., $C_2=kC_1$, where k is the ratio of the distance between the neutral plane and the ceiling to the distance between the carriage top and the ceiling, which represents the air entrainment difference in the two directions.

Equation (4) can be rewritten as:

$$Sv_f = \pi \ell_T \ell_L \sqrt{\left(\Delta T_f / T_\infty\right) gZ} \in \varphi \frac{\dot{Q}_{ex}}{\rho_f \Delta H_c} \tag{6}$$

where, $\varphi = \frac{\int_Z^{H_f} \pi \ell_T \ell_L dz}{\int_0^{H_f} \pi \ell_T \ell_L dz}$, ΔH_c is combustion heat of the fuel (kJ/kg), ρ_f is the density of ejected flame (kg/m^3), H_f is the ejected flame height for free condition without tunnel ceiling (m).

Hence, the dimensionless form is

$$\frac{\ell_L \ell_T}{\ell_1 \ell_2} \in \varphi \frac{\dot{Q}_{ex}}{\ell_1 \ell_2 \rho_f \Delta H_c \sqrt{\left(\Delta T_f / T_\infty\right) gZ}} \tag{7}$$

where φ can be integrated based on the assumption that the cross-section of flame is elliptical. It gives:

$$\varphi = \frac{\int_Z^{H_f} \pi \ell_T \ell_L dz}{\int_0^{H_f} \pi \ell_T \ell_L dz} = \frac{\frac{\pi}{4}(\ell_1 \ell_2)(H_f - Z) + \frac{\pi}{4}(\ell_1 C_1 + \ell_2 C_2)\left[(H_f)^2 - (Z)^2\right] + \frac{\pi}{3} C_1 C_2 \left[(H_f)^3 - (Z)^3\right]}{\frac{\pi}{4}(\ell_1 \ell_2)(H_f) + \frac{\pi}{4}(\ell_1 C_1 + \ell_2 C_2)(H_f)^2 + \frac{\pi}{3} C_1 C_2 (H_f)^3} \tag{8}$$

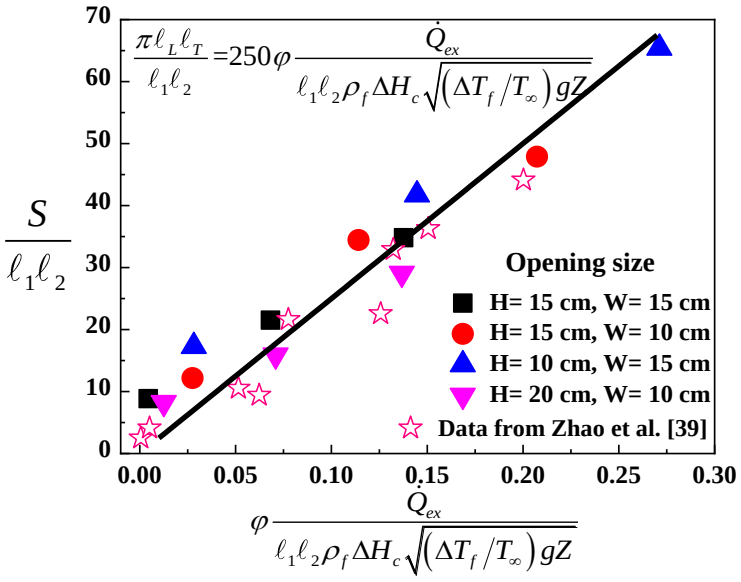

Figure 10. A relationship between the measured flame extension areas under the channel ceiling induced by the ejected flame from the carriage and the revised fire heat release rates.

Figure 10 plots the dimensionless flame extension area against the dimensionless HRR for all the cases when the carriage is located at the transverse centreline. Combining Eqs. (6), (7), (8) and Fig. 10, it can be found that the dimensionless flame extension area is proportional to the dimensionless excess HRR, and equation (9) is obtained. Since $\dot{Q}_{ex} = \dot{Q} - \dot{Q}_{inside}$, $\dot{Q}_{inside}$ is a fixed value after the fire completely spilled out, the excess HRR is hence proportional to the total HRR. The results confirm that the dimensionless flame extension area is proportional to the dimensionless HRR and a correlation can be determined based on the best fit of the data as shown in Eq. (9) and Figure 10. For comparison purpose, comparison has also been made between the predictions and the measurements from previous work studying buoyant opening spill flames beneath a horizontal projection, which were not used in the derivation of the correlation [39]. The relatively good agreement further illustrates validity of the derived correlation although further validations against more experimental data or numerical simulations in the future would provide more insight into the

flame extension under the ceiling.

$$\frac{S}{\ell_1\ell_2}=\frac{\pi\ell_L\ell_T}{\ell_1\ell_2}=3.14*80\varphi\frac{\dot{Q}_{ex}}{\ell_1\ell_2\rho_f\Delta H_c\sqrt{\left(\Delta T_f/T_\infty\right)gZ}}=250\varphi\frac{\dot{Q}_{ex}}{\ell_1\ell_2\rho_f\Delta H_c\sqrt{\left(\Delta T_f/T_\infty\right)gZ}} \quad (9)$$

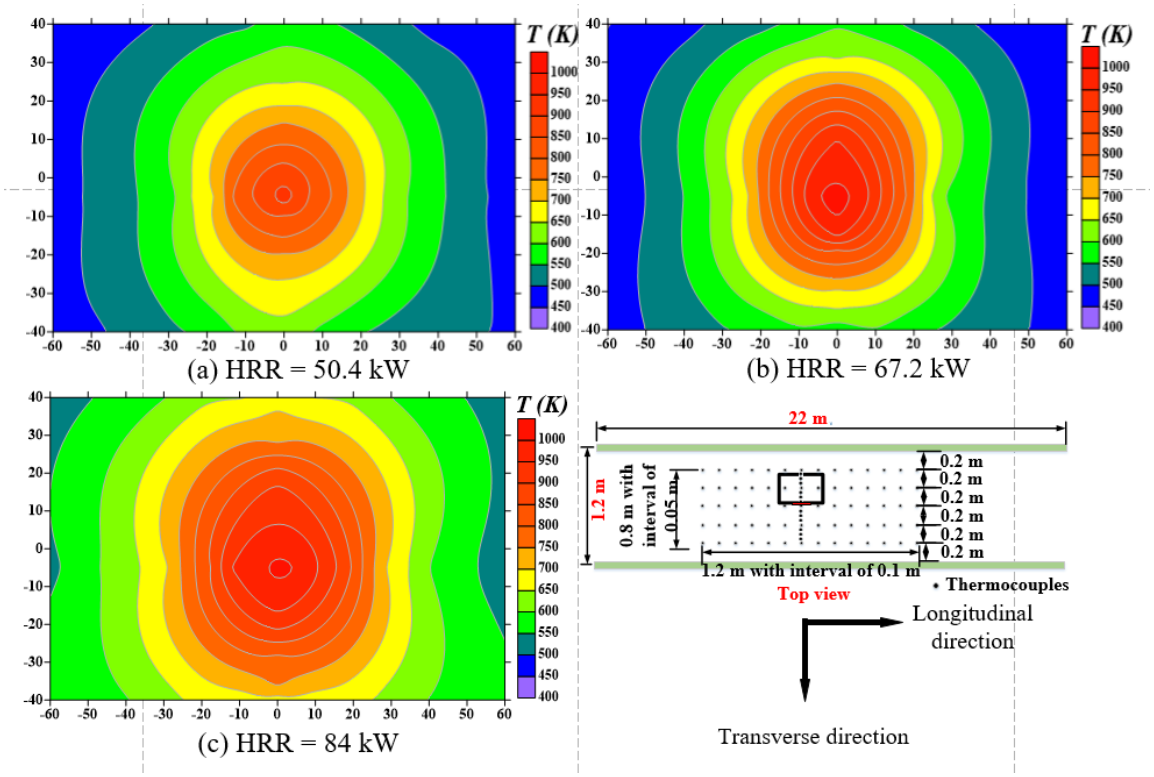

Figure 11. Two-dimensional ceiling temperature for opening size of *H*=15, *W*=15. *D*=60 cm.

The flame extension area on the ceiling, which can be correlated by Eq. (9), has direct relevance to the potential fire damages to the channel structure. Due to the limited space in the channel, the length of the ceiling flame is usually longer than that of an open flame or indoor fire. This horizontal of the ceiling flame increases the risk of fire spread inside the channel and affect other adjacent objects, e.g. the channel structure and adjacent carriages. Such impact can result in cascading effects. Based on the Froude similarity criterion [33], the tested fire is equivalent to a car or carriage fire in practical channel/tunnel, the above correlations for the longitudinal and transverse flame extensions on the

ceiling and the flame extension area can hence be used to estimate the potential ceiling flame extension areas in practical situations, and assist the design optimization of window openings to reduce potential impact of the fire by limiting its spread on the ceiling.

Figure 11 presents the two-dimensional ceiling temperature for opening size of H=15 and W=15, where the thermocouple trees were set between 20 to 60 cm in the transverse direction and from 0 to 60 cm in the longitudinal direction (the position of the carriage can be seen from the top view). The maximum temperature occurs at the rear of carriage and close to the opening, which is consistent with flame extension characteristics shown in Figure 7. The flame extension lengths can be estimated based on the temperature rise (800 K) at the intersection of the intermittent flame and plume regions of buoyant gas diffusion flames [40]. For example, for the case in Figure 11c (HRR=84 kW), the transverse flame extension length determined from the temperature measurements is approximately 50 cm and longitudinal flame extension length 44 cm, which are in good agreement with the predicted values using Eqs. (3a) and (3b) which gave ℓ_T=52.5cm, ℓ_L=47.5cm, respectively. By applying the similarity scaling of Quintiere [33], the present data was also used to determine the flame lengths in the full-scale model. For the case in Figure 9a, the equivalent ceiling flame extension lengths for an ejected flame with a heat release rate of 2.95 MW in a full-scale tunnel was estimated as 3.55 m and 4.41 m in the transverse and longitudinal directions, respectively.

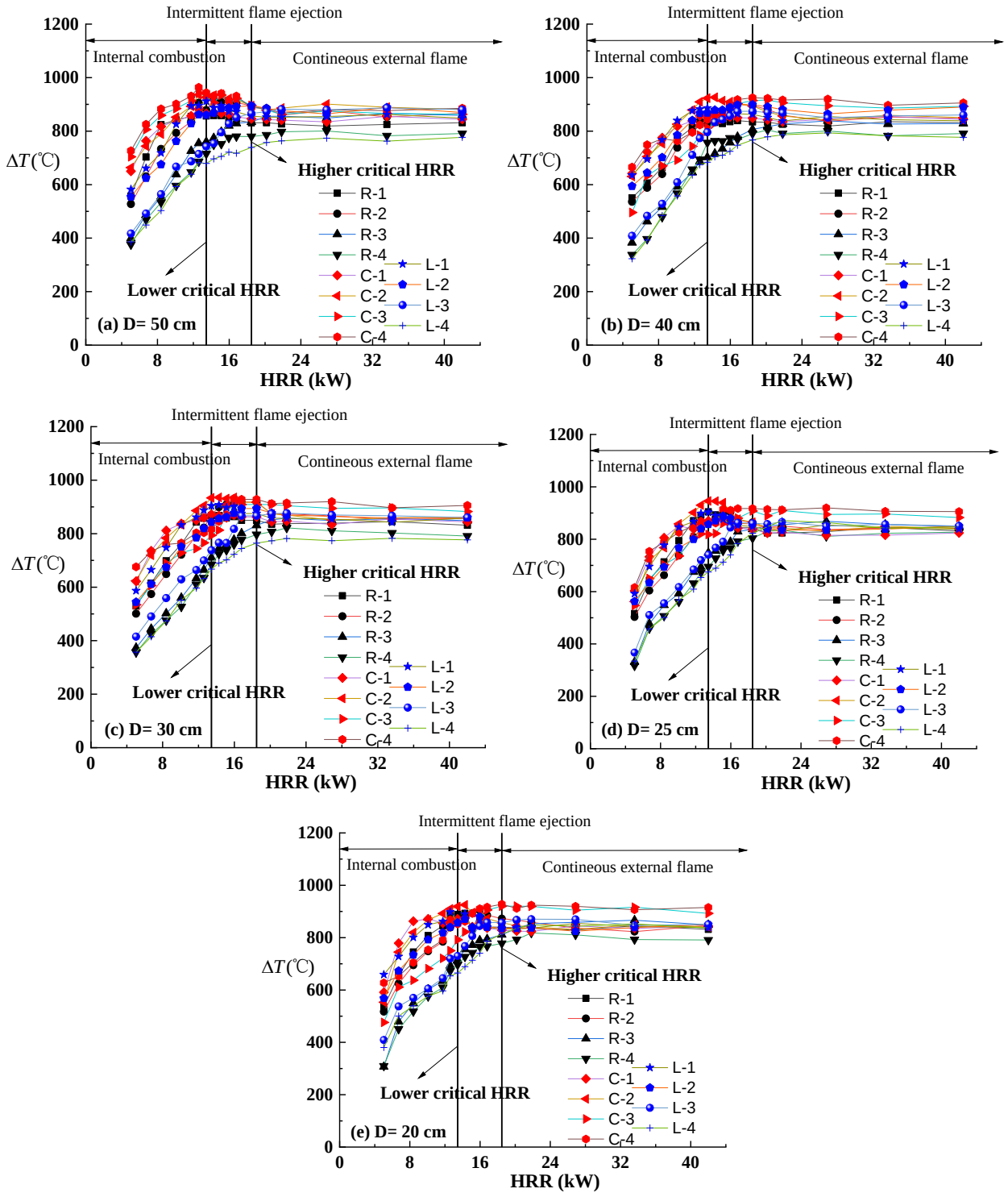

Figure 12. Temperature evolution inside the enclosure under different heat release rates and different sidewall to opening distance (opening size is 15 cm × 15 cm).

3.2 Critical heat release rate and ceiling extension of the ejected flame induced by carriage fires under sidewall effect in channel

Analysis is firstly conducted to establish the effect of the sidewall on the HRR inside the enclosure. Figure 12 shows the temperature evolution inside the enclosure with different HRRs and sidewall to opening distances (opening size is 15 cm ×15 cm). The results indicate that the sidewall had almost no effect on the temperature inside the enclosure and the critical HRR. This is because the critical heat release rate before external burning and the associated gas temperature inside the enclosure depend primarily on the opening factor. Figure 13 further indicates that the mean critical $\dot{Q}_{inside}$ was also not affected by the increase of sidewall-to-opening distance *D*.

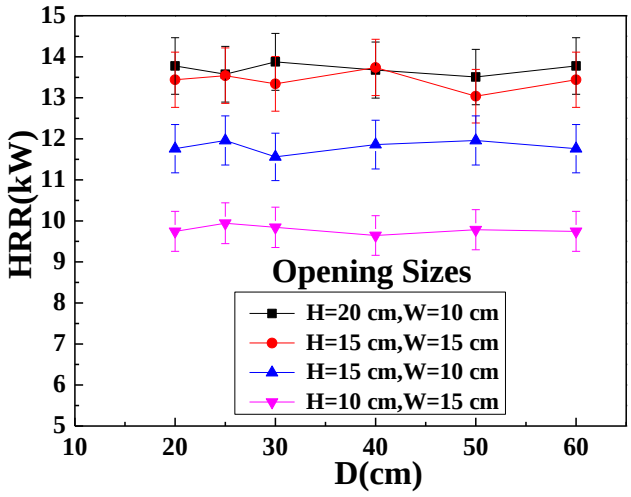

Figure 13. The variation of the mean critical HRR with different sidewall-to-opening distance.

Figure 14 depicts the side view of the mean flame contour images of the ejected flame with an opening of *H*=15 cm, *W*=10 cm for different *D* values (HRR=67.2 kW). These were obtained by the image processing procedure described in Section 2. The transverse and longitudinal flame extension lengths under channel ceiling can be obtained from the measurements of these images.

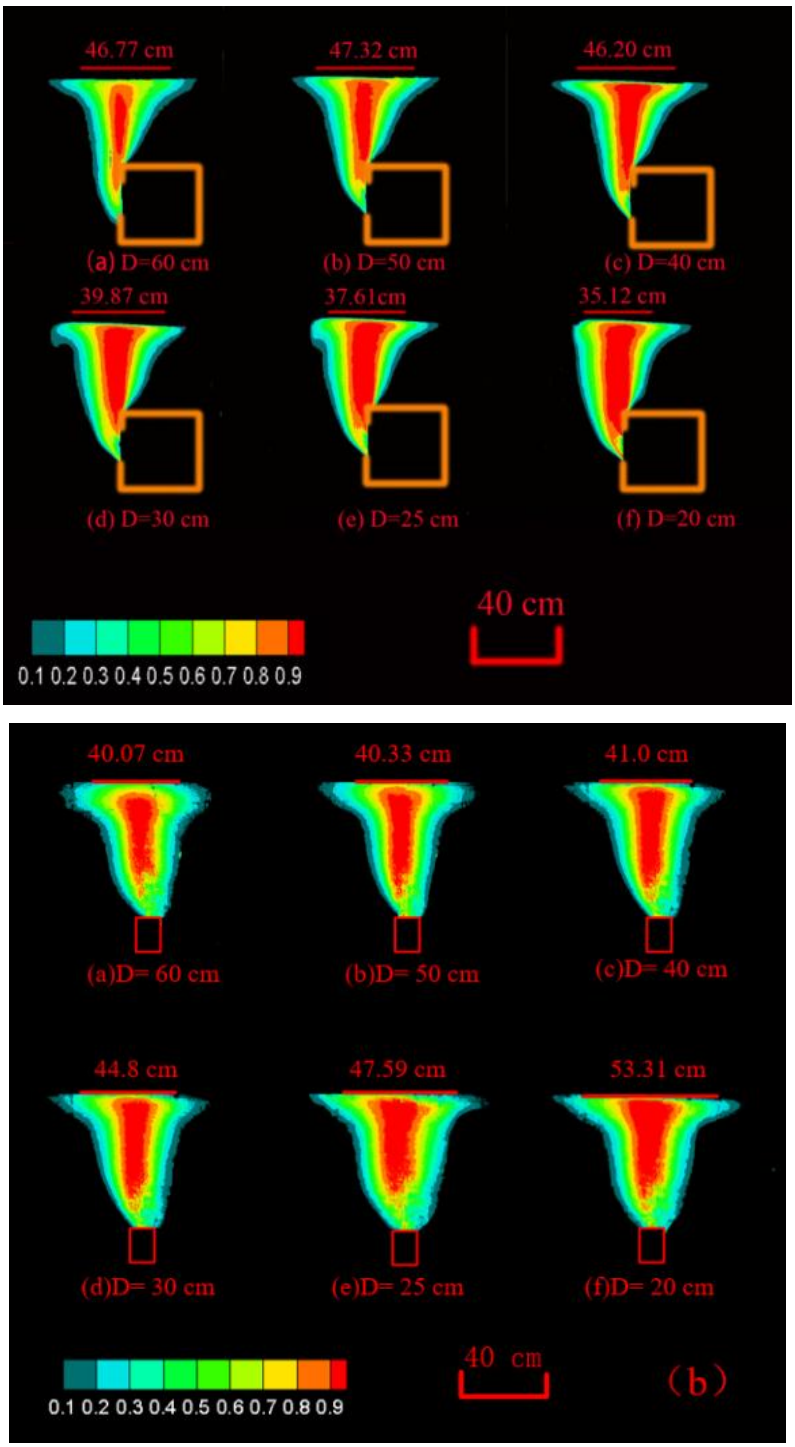

Figure 14. Contour images of the ejected flames with opening of *H*=15 cm, *W*=10 cm for different sidewall-to-opening distances: (a) transverse flame extension length; (b) longitudinal flame extension length.

These results show that with the decrease of the sidewall-to-opening distance, the transverse flame extension length under channel ceiling decreases whereas the longitudinal flame extension length increases. The changes were most significant when D is less than 30 cm. These trends are different from those observed in previous wall fires or corner fires, in which the flame extension length beneath the ceiling firstly increases with the decrease of source-sidewall-to-opening distance, and then decrease slightly when the fire source is against the wall in the channel fires (its channel height is 0.88 m and width is 2 m) [41]. The safety implication is that small opening to sidewall-to-opening distances would result in faster ceiling jet flame spread in the longitudinal direction with the potential for faster fire spread from the original fire carriage to the others.

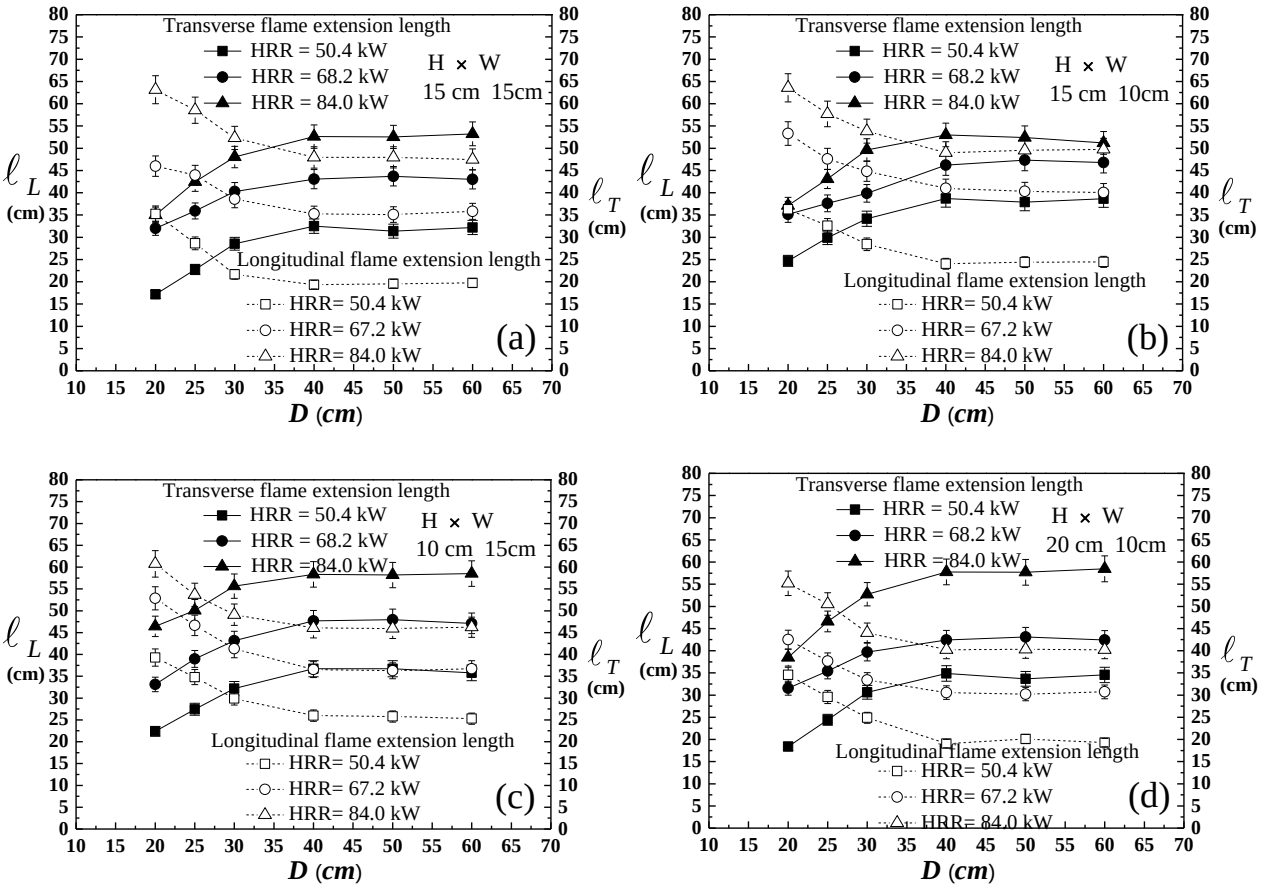

Figure 15. Flame extension lengths under the ceiling with different sidewall-to-opening distance.

Figure 15 shows the variation of flame extension length under the channel ceiling with different sidewall-to-opening distances. It was found that, when D=20 cm, the longitudinal flame extension length is more than twice that in the transverse direction. When the opening of the carriage is located at the centreline of the channel, the sidewalls have almost no restriction on air entrainment. Since the flame is ejected from the transverse direction of the channel, the initial velocity of the ejected flame in the transverse direction is greater than that in the longitudinal direction and hence the lateral flame extension length is greater than that in the longitudinal direction. When the flame gradually approaches the sidewall, due to the restriction of air entrainment by the sidewall, the flame is limited by the sidewall and forced to extend in the longitudinal direction, resulting in gradual increase of the longitudinal flame extension length and eventually became greater than the lateral direction. Therefore, as the distance changes, the flame extension length in different directions will change. For a ceiling jet induced by ejected flames, when this sidewall-to-opening distance D decrease gradually, the air entrainment from the front is partially restricted, resulting in the change of flame extension length under the channel ceiling in both longitudinal and transverse directions, as shown in Fig. 16. This effect will be analysed in a physical model to characterize the effect of sidewall constraint on air entrainment.

In the presence of a sidewall, the sidewall-to-opening distance D plays a key role in flame extension length, the flame extension length induced by the ejected flame from a carriage in a channel should be a function of both the excess HRR and sidewall-to-opening distance (D).

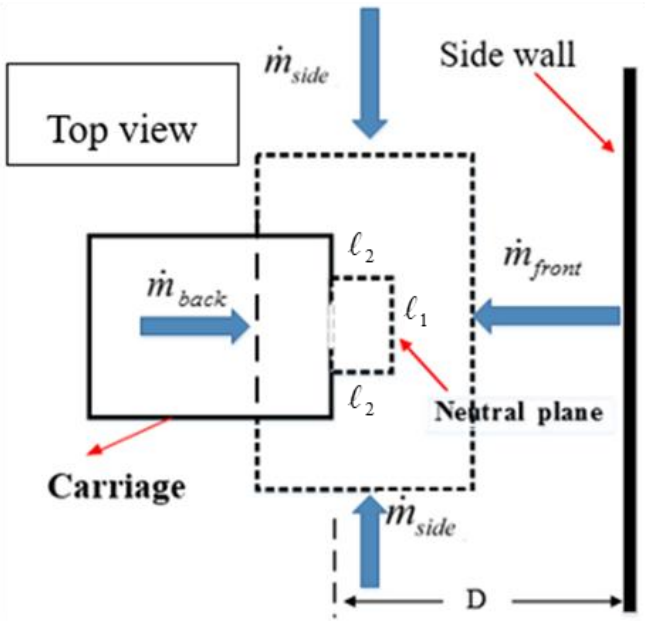

Figure 16. Physical features to characterize the effect of sidewall constraint on air entrainment for ejected flames.

In diffusion flames like fires, combustion is sustained through entrainment of fresh air by the fire plume. The air entrainment mass rate $m_{entrainment}$ can be expressed by Eq. (10) following [8, 42]:

$$m_{entrainment}=\rho_a v_a S_{entrainment} \tag{10}$$

where the ρ_a is the air density (kg/m^3), v_a is the air entrainment velocity ($v_a=\sqrt{g\bar{H}}$, $\bar{H}$ is the channel height (m), $S_{entrainment}$ is the air entrainment area(m^2).

As shown in Fig. 16 and Fig. 1b, the air entrainment area of the ejected fire plume can be approximated by as:

$$S_{entrainment}=S_{front}+S_{side} \tag{11a}$$

$$S_{front}=S_{front}\left|\begin{matrix}H_{carriage}\\H_{neutral}\end{matrix}\right.+S_{front}\left|\begin{matrix}H_{tunnel}\\H_{carriage}\end{matrix}\right. \tag{11b}$$

$$S_{front}=S_{front}\left|\begin{matrix}H_{carriage}\\H_{neutral}\end{matrix}\right.+S_{front}\left|\begin{matrix}H_{tunnel}\\H_{carriage}\end{matrix}\right. \tag{11c}$$

where the S_{front} is the air entrainment area from the front of the opening sizes, S_{side} is the air entrainment area from the side direction of the opening sizes, $H_{neutral}$ is the height of the neutral plane (m), $H_{carriage}$ is the height of the carriage (m), $\bar{H}$ is the channel height (m). Between the $H_{neutral}$ and the $H_{carriage}$, the S_{front} was from one side. However, the S_{front} was from two side between the $H_{carriage}$ and the $\bar{H}$. And the S_{side} was always from two side.

When the ejected flame was not restricted by the channel sidewall, the air entrainment area of the ejected flame can be calculated as:

$$S_{entrainment,\infty} = (2\ell_2 + \ell_1)\begin{vmatrix} H_c \\ H_n \end{vmatrix} + (2\ell_2 + 2\ell_1)\begin{vmatrix} H_t \\ H_c \end{vmatrix} \approx \frac{1}{6} H(10\ell_2 + 8\ell_1) \tag{12}$$

where the l_1 is characteristic width of rectangular fire source (parallel to carriage front wall), m; l_2 is characteristic length of rectangular fire source (perpendicular to carriage front wall).

When the ejected fire from carriage opening was restricted by the channel sidewall, the air entrainment area can be expressed as:

$$S_{entrainment,D} = (2l_2 + \lambda l_1)\begin{vmatrix} H_c \\ H_n \end{vmatrix} + (2l_2 + (1+\lambda l_1)\begin{vmatrix} H_t \\ H_c \end{vmatrix} \approx \frac{1}{6} H(10l_2 + (3+5\lambda)l_1) \tag{13}$$

where the λ is a coefficient of air entrainment due to the influence of different sidewall-to-opening distances D.

It is proposed to introduce an air entrainment correction factor K of the ejected flame from the carriage opening, which can be expressed as:

$$K = \frac{m_{entrainment,D}}{m_{entrainment,\infty}} = \frac{\rho_a v_a S_{entrainment,D}}{\rho_a v_a S_{entrainment,\infty}} = \frac{S_{entrainment,D}}{S_{entrainment,\infty}} \approx \frac{13}{18} + \frac{5\lambda}{18} \tag{14}$$

Equation (14) shows that the air entrainment correction factor can be correlated by a coefficient λ. Figures 13 and 14 indicates that when the sidewall-to-opening distance *D* is between the 40 cm and 60 cm, its effect on air entrainment is negligible, the flame extension length can be calculated by Eq.

(3). However, the air entrainment from the front is partially restricted when this sidewall-to-opening distance *D* decrease gradually. Moreover, the flame extension length expands with the decrease of the sidewall-to-opening distance. Hence, when the air entrainment restricted by the sidewall, the flame extension length can be expressed using either Eq. (15a) or (15b). The critical point was effect by the sidewall distance D and the characteristic length of rectangular fire source ℓ_1.

$$(\ell_L + Z)/\ell_1 = 3.40\dot{Q}_{ex}^{*2/5} = a\dot{Q}_{ex}^{*2/5}e^{K_L} \tag{15a}$$

$$(\ell_T + Z)/\ell_1 = 3.75\dot{Q}_{ex}^{*2/5} = b\dot{Q}_{ex}^{*2/5}e^{K_T} \tag{15b}$$

where K_L is the longitudinal air entrainment correction factor ($K_L = \frac{13}{18} + \frac{5\lambda_L}{18}$), and K_T is the transverse air entrainment correction factor $K_T = \frac{13}{18} + \frac{5\lambda_T}{18}$.

When the air entrainment hardly be restricted by the channel side wall D. The air entrainment correction factor is $K_L = K_T = 1$. According to the $K_L = K_T = 1$, equations (15a) and (15b) can be rewritten as Eqs. (16a) and (16b):

$$(\ell_L + Z)/\ell_1 = \frac{3.40}{e}\dot{Q}_{ex}^{*2/5}e^{k_L} = 1.25\dot{Q}_{ex}^{*2/5}e^{K_L} \tag{16a}$$

$$(\ell_T + Z)/\ell_1 = \frac{3.75}{e}\dot{Q}_{ex}^{*2/5}e^{k_T} = 1.38\dot{Q}_{ex}^{*2/5}e^{K_T} \tag{16b}$$

In order to account for the effect of air entrainment λ, as the result shown in Figure 13, with the decrease of channel sidewall-to-opening distance, the air entrainment λ remained approximately constant at first, then decreased with the decrease of sidewall-to-opening distance. The sidewall-to-opening distance D and the characteristic length ℓ_1 should hence be incorporated in the calculation of λ. Moreover, λ should 1 when D is more than a threshold value related to the characteristic length ℓ_1. If the threshold value is $m\ell_1$. A piecewise function is introduced in Eq. (17) about transverse air entrainment coefficient λ_L and longitudinal air entrainment coefficient λ_T while the value of m can

be obtained from analysis of the measurements.

$$\lambda_L = \begin{cases} (\dfrac{D}{m\ell_1})^n, 0 < D \le m\ell_1, \\ 1, D > m\ell_1 \end{cases} \tag{17a}$$

$$\lambda_T = \begin{cases} (\dfrac{D}{m\ell_1})^{-n}, 0 < D \le m\ell_1, \\ 1, D > m\ell_1 \end{cases} \tag{17b}$$

When $D \le m\ell_1$, the $\lambda_L = (D/m\ell_1)^n$ in the transverse flame extension length and $\lambda_L = (D/m\ell_1)^{-n}$ in the longitudinal flame extension length. When $D > m\ell_1, \lambda = \lambda_L = \lambda_T = 1$. In this paper, the critical point approximately is 40 cm, the characteristic length ℓ_1 vary from 11.8 to 15.2, so m is $\dfrac{40}{(11.8+15.2)/2} = 3$.

A piecewise function was proposed to describe the variation of flame extension length under the channel ceiling with different sidewall-to-opening distances. When the sidewall-to-opening distance is more than $3\ell_1$, the effect of the sidewall-to-opening distance is negligible, and the corresponding correlations of flame extension lengths are shown in Eq. (3). The dimensionless flame extension lengths induced by carriage fires under sidewall effect in channel ($0<D \le 3\ell_1$) are plotted in Fig. 17, along with the experimental data on horizontal flame extension distance (without sidewall effect) under ceiling induced by ejected fire plume with various heat release rates [39]. Both sets of data have similar trends, and the correlations of dimensionless flame extension length induced by carriage fires under sidewall effect in channel for both directions were finally obtained, n=2/3, as shown in Eq. (18), which predicts well both the present experimental data and data in [39] which were not used in the above derivation, with R^2 values of 0.96 and 0.97 for longitudinal and transverse flame extension lengths, respectively.

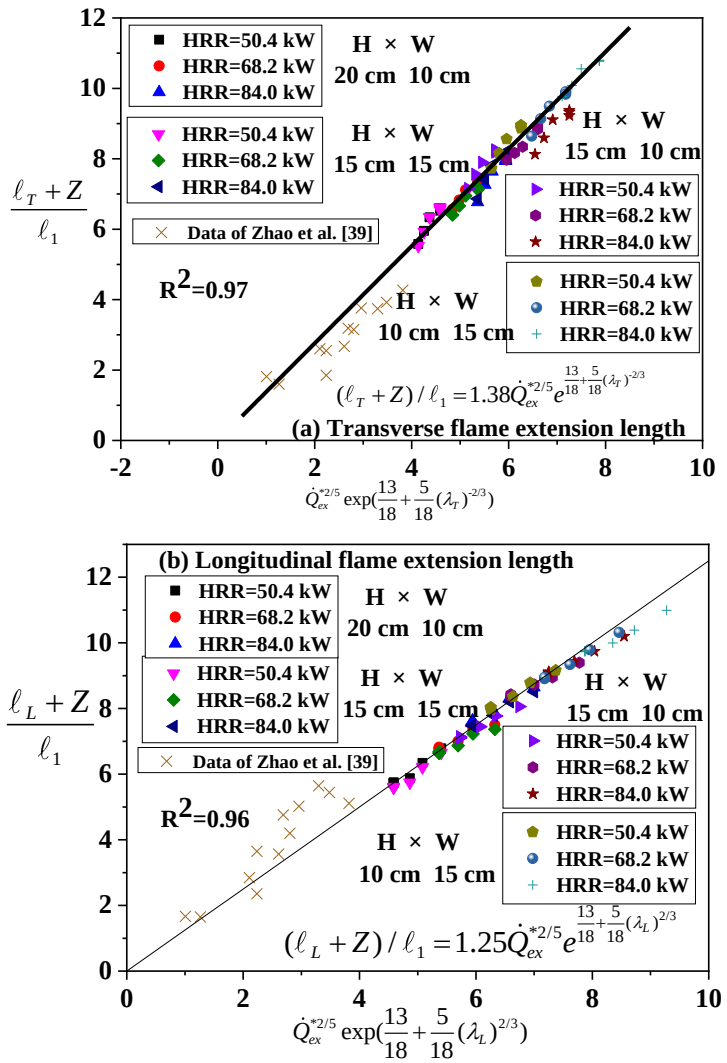

Figure 17. Correlation of dimensionless flame extension length induced by carriage fires under sidewall effect in channel.

Longitudinal flame extension length: $(\ell_L + Z)/\ell_1 = 1.25\dot{Q}_{ex}^{*2/5} e^{\frac{13}{18}+\frac{5}{18}\lambda^{2/3}}$ (18a)

Transverse flame extension length: $(\ell_T + Z)/\ell_1 = 1.38\dot{Q}_{ex}^{*2/5} e^{\frac{13}{18}+\frac{5}{18}\lambda^{-2/3}}$ (18b)

where the air entrainment λ can be rewritten as Eq. (19) .

Longitudinal air entrainment coefficient: $\lambda_L = \begin{cases} (\frac{D}{3\ell_1})^{2/3}, 0 < D \le 3\ell_1, \\ 1, D > 3\ell_1 \end{cases}$ (19a)

Transverse air entrainment coefficient: $\lambda_T = \begin{cases} (\frac{D}{3\ell_1})^{-2/3}, 0 < D \le 3\ell_1, \\ 1, D > 3\ell_1 \end{cases}$ (19b)

4. Conclusions

Experimental studies were firstly conducted to gain insight of flame ejection from enclosure fires. The variations of the critical HRR which distinguish the three burning stages of fuel-controlled enclosure fires with the ventilation factor were examined when the carriage was at the centre of the channel. It was found that the critical lower and upper HRRs of intermittent flame ejection increased with the increase of the ventilation factor. The lower critical HRR gradually approaches the value predicted by the formula of Lee et al. [27] when the ventilation factor is sufficiently large. The transverse flame extension length is larger than the longitudinal flame extension length due to the restriction of air entrainment by the channel sidewall. Correlations for the longitudinal and transverse flame extension lengths and flame extension area beneath the ceiling were proposed.

Subsequently, the effects of sidewall on the flame extension characteristics of ejected flames from a carriage in the channel were experimentally investigated. The sidewall-to-opening distance was found to have considerable influence on the ceiling flame extension lengths. Small sidewall-to-opening distance resulted in faster ceiling flame spread in the longitudinal direction with the potential for faster fire spread from the original fire carriage to the others. New correlations have been proposed for the longitudinal and transverse flame extension lengths.

To demonstrate their potential for fire safety engineering applications, all the correlations developed have been compared with the present measurements as well as some published data not used in their derivations. These dimensionless correlations can be used to estimate ceiling flame extension lengths and areas under different sidewall-to-opening distances in practical situations; and assist the design optimization of window openings and their distance to the sidewall to reduce potential impact of the fire by limiting its spread on the ceiling.

Acknowledgements

This work was supported jointly by National Nature Science Funds of China under Grant No. 51776060, and Fundamental Research Funds for the Central Universities under Grant No. PA2019GDQT0014.

References

[1]. A. Lonnermark, H. Ingason, Fire spread and flame length in large-scale tunnel fires, *Fire Technol.* 42 (4) (2006) 283–302.

[2]. B.Y. Lattimer, Heat fluxes and flame lengths from fires under ceilings, *Fire Technol.,* 49 (2013) 269-291.

[3]. R.L. Alpert, Turbulent ceiling-jet induced by large-scale fires, *Combust. Sci. Technol.* 11 (1975) 197-213.

[4]. H.Z. You, G.M. Faeth, Ceiling heat transfer during fire plume and fire impingement, *Fire Mater.* 3 (3) (1979) 140–147.

[5]. W.G. Weng, Y. Hasemi, Heat transfer to an unconfined ceiling from an impinging buoyant diffusion flame, *Heat Mass Transf.* 42 (7) (2006) 652–659.

[6]. H.W. Ding, J.G. Quintiere, An integral model for turbulent flame radial lengths under a ceiling, *Fire Saf. J.* 52 (2012) 25–33.

[7]. X.C. Zhang, L.H. Hu, W. Zhu, X.L. Zhang, L.Z. Yang, Flame extension length and temperature profile in thermal impinging flow of buoyant round jet upon a horizontal plate, *Appl. Therm. Eng.* 73 (2014) 15–22.

[8]. J.G. Quintiere, Fundamentals of Fire Phenomena, John Wiley & Sons, Ltd., West Sussex, England,

2006.

[9]. D. Drysdale, An Introduction to Fire Dynamics, (third ed.), John Wiley & Sons, Ltd., Chichester, UK, 2011.

[10]. E.E. Zukoski, in: G. Cox, (Ed.), Combustion Fundamentals of Fire, Academic Press, London, 1995.

[11]. Y. Hasemi, T. Tokunaga, Some experimental aspects of turbulent diffusion flames and buoyant plumes from fire sources against a wall and in a corner of walls, *Combust. Sci. Technol.* 40 (1984) 1-18.

[12]. M. Poreh, G. Garrad, A study of wall and corner fire plumes, *Fire Saf. J.* 34 (2000) 81-98.

[13]. W. Takahashi, H. Tanaka, Flame and plume behavior in and near a corner of walls, Fire safety science- proceedings of the fifth international symposium, (1997)261-271.

[14]. T. Mizuno, K. Kawagoe, Burning Behaviour of Upholstered Chairs Part 3, Flame and Plume Characteristics in Fire Test, *Fire Sci. Technol.* 6 (1986) 29-37.

[15]. C. Qian, H. Ishida, K. Saito, Upward flame spread along PMMA vertical corner walls part II: mechanism of m shape pyrolysis front formation, *Combust. Flame*, 99 (1994) 331-338,

[16]. F. Tang, L.J. Li, Q. Wang, Q. Shi, Effect of crosswind on near-wall buoyant turbulent diffusion flame length and tilt, *Fuel* 186 (2016) 350-357.

[17]. J. Ji, C.G. Fan, Y.Z. Li, H. Ingason, J.H. Sun, Experimental study of non-monotonous sidewall effect on flame characteristics and burning rate of n-heptane pool fires, *Fuel,* 145 (2015) 228–233.

[18]. N. Ren, Y. Wang, S. Vilfayeau, A. Trouvé, Large eddy simulation of turbulent vertical wall fires supplied with gaseous fuel through porous burners, *Combust. Flame*, 169(2016)194-208.

[19]. T.N. Zhou, Y.P. He, X. Lin, X.H. Wang, J. Wang, Influence of constraint effect of sidewall on

maximum smoke temperature distribution under a tunnel ceiling, *Appl. Therm. Eng.* 112 (2017) 932–941.

[20]. Q. Wang, J. Yan, L.M. Shi, F. Tang, An experimental investigation on oscillating length scale of gas pipeline leakage flame restricted by parallel sidewalls, *Combust. Flame*, 215 (2020) 252-258.

[21]. D. Zeinali, S. Verstockt, T. Beji, G. Maragkos, J. Degroote, B. Merci, Experimental study of corner fires—Part I: inert panel tests, *Combust. Flame*, 189 (2018) 472–490.

[22]. D. Zeinali, S. Verstockt, T. Beji, G. Maragkos, J. Degroote, B. Merci, Experimental study of corner fires—Part II: flame spread over MDF panels, *Combust. Flame*, 189 (2018) 491–505.

[23]. L.H. Hu, K.H. Lu, F. Tang, M. Delichatsios, L.H. He, A global non-dimensional factor characterizing side wall constraint effect on facade flame entrainment and flame height from opening of compartment fires, *Inter. J. Heat Mass Transf.* 75 (2014) 122-129.

[24]. J. Ji, K. Harada, Y. Ohmiya, M. Noaki, Tilt of flame from an item burning close to a wall, *Fire techno.,* 54 (2018) pages1383–1404.

[25]. X.L. Zhang, L.H. Hu, M.A. Delichastios, J.P. Zhang, Experimental study and analysis on flame lengths induced by wall-attached fire impinging upon an inclined ceiling, *Proc Combust Inst*, 37 (3) (2019) 3879-3887

[26]. B. Merci, T. Beji, Fluid mechanics aspects of fire and smoke dynamics in enclosures, CRC Press, 2016.

[27]. Y.P. Lee, M.A. Delichatsios, G. Silcock, Heat fluxes and flame heights in facades from fires in enclosures of varying geometry, *Proc. Combust. Inst.* 31 (2007) 2521–2528.

[28]. K. Himoto, T. Tsuchihashi, Y. Tanaka, T. Tanaka, Modeling thermal behaviors of window

flame ejected from a fire compartment, *Fire Saf. J.* 44 (2009) 230–240.

[29]. K.H. Lu, L.H. Hu, F. Tang, L.H. He, X.C. Zhang, Z.W. Qiu, Experimental investigation on window ejected facade flame heights with different constraint side wall lengths and global correlation, *Inter. J. Heat Mass Transf.* 78 (2014) 17–24.

[30]. Y. Ohmiya, T. Tanaka, T. Wakamatsu, A room fire model for predicting fire spread by external flames, *Fire Sci. Technol.,* 18 (1998) 11-21.

[31]. M.A. Delichatsios, Y.P. Lee, P. Tofilo, A new correlation for gas temperature inside a burning enclosure, *Fire Safety J.,* 44 (2009) 1003-1009.

[32]. L.H. Hu, X.P. Sun, X.L. Zhang, F. Ren, Facade flame height and horizontal extending distance from opening of compartment fire with external sideward wind, *Proc. Combust. Inst.,* 37 (2019) 3859-3867.

[33]. J. G. Quintiere, Scaling applications in fire research, *Fire Saf. J.* 15 (1989) 3-29.

[34]. N. Otsu, A threshold selection method from gray-level histograms, IEEE T Syst Man CY-S, 9 (1979) 62 – 6.

[35]. L.G. Blevins, W.M. Pitts, Modeling of bare and aspirated thermocouples in compartment fires, *Fire Saf. J.* 33 (4) (1999) 239–259.

[36]. L.H. Hu, K.H. Lu, M. Delichatsios, L.H. He, F. Tang, An experimental investigation and statistical characterization of intermittent flame ejecting behavior of enclosure fires with an opening, *Combust. Flame* 159 (2012) 1178-1184.

[37]. H.Y. Wang, P. Joulain, Three-dimensional modeling for prediction of wall fires with buoyancy-induced flow along a vertical rectangular channel, *Combust. Flame* 105 (1996) 391-406.

[38]. J.G. Quintiere, B.S. Grove, A unified analysis for fire plumes, *Symp. (Inter.) Combust.* 27 (1998) 2757–2766.

[39]. C. Zhao, D. Yang, F. Tang, Y.Q. Jiang, Buoyant opening spill flame behaviors beneath a horizontal projection induced by a compartment fire, *Exp. Heat Transfer* 32 (2019) 284–301.

[40]. B. J. McCaffrey, Purely buoyant diffusion flames: some experimental results. Report No. NBSIR 79-1910, 1979. National Bureau of Standards Interagency.

[41]. Z.H. Gao, J. Ji, H.X. Wan, K.Y. Li, J.H. Sun, An investigation of the detailed flame shape and flame length under the ceiling of a channel, *Proc. Combust. Inst.* 35 (2015) 2657–2664.

[42]. B. Karlsson, J.G. Quintiere, Enclosure Fire Dynamics, CRC Press (2000).